Journal of Nanophotonics

Nanophotonics.SPIEDigitalLibrary.org

# Surface-to-volume ratio controls the radiation of stratified plasmonic antennas

Banafsheh Abasahl
Christian Santschi
Olivier J. F. Martin

SPIE.

Banafsheh Abasahl, Christian Santschi, Olivier J. F. Martin, "Surface-to-volume ratio controls the radiation of stratified plasmonic antennas," *J. Nanophoton.* **11**(4), 046006 (2017), doi: 10.1117/1.JNP.11.046006.

# Surface-to-volume ratio controls the radiation of stratified plasmonic antennas

**Banafsheh Abasahl,[†] Christian Santschi, and Olivier J. F. Martin[*]**
Swiss Federal Institute of Technology Lausanne (EPFL), Nanophotonics and Metrology Laboratory, Lausanne, Switzerland

**Abstract.** Surface plasmons are excited at a metal/dielectric interface, through the coupling between conduction electrons and incident photons. The surface plasmon generation is therefore strongly determined by the accessibility of the surface to the incoming electromagnetic field. We demonstrate the role of this surface for plasmonic nanoantennas with identical volumes and resonant lengths. An antenna is stratified parallel to the plane of its main dipolar resonance axis and the influence of the number of layers and the spacing between them on the optical properties of the antenna are investigated experimentally. We show that increasing the number of layers and, hence, increasing the total accessible surface of the antenna, results in an enhanced scattering cross section and a redshift which indicates that lower energy photons are required to couple to the metal electrons. In particular, the far-field enhancement observed for double-layer nanostructures suggests that standard single-layer metal deposition can be easily and advantageously substituted with metal/dielectric/metal deposition to boost light scattered by a plasmonic antenna.  [DOI: 10.1117/1.JNP.11.046006]

**Keywords:** plasmonics; optical antennas; materials; scattering; lumped circuit; nanotechnology.

Paper 17126L received Aug. 23, 2017; accepted for publication Sep. 27, 2017; published online Oct. 30, 2017.

## 1 Introduction

Plasmonic nanoantennas can localize light to a subdiffraction-limited spot[1–4] and reradiate it into the far-field. In the so-called hot spot, the field intensity is enhanced by several orders of magnitude at the resonance wavelength.[5–8] These fundamental properties stem from the localized surface plasmon resonances. Additional features can be enabled by engineering the shape of nanoantennas, such as the broadband response of bowtie antennas,[9] the directionality of nano Yagi-Uda antennas,[10] and the ultralocalized and enhanced near-fields of gap antennas.[11–23] Several elements determine the field enhancement of a nanoantenna: strong photon–electron coupling at the metal surface, capacitive coupling at the disruption of the induced current path in the gap or at the end of the structure, and coupling to the surrounding environment. Although at optical frequencies the lateral dimensions of a nanoantenna are much smaller than the bulk penetration depth, the electric current density is not distributed uniformly, but rather it is higher at the surface of the structure. An example of such an electric field distribution can be seen in Fig. 1(a) for a nanorod, where the inside of the structure is depleted from the field intensity, while the latter increases close to the surface. In this article, the effect of the strong photon–electron interaction at the surface of a nanoantenna is investigated for such a nanorod geometry, Fig. 1(a). Specifically, the overall surface of the nanoantenna is altered while maintaining the total metal volume. To this end, the nanorod antenna shown in Fig. 1(a) is stratified according to Figs. 1(b) and 1(c). The antenna is excited with the electric field polarized along the $x$-direction, so that the dielectric interlayers added by the stratification do not interrupt the current path of the main dipole resonance. Each nanoantenna shown in Fig. 1 has the same

*Address all correspondence to: Olivier J. F. Martin, E-mail: olivier.martin@epfl.ch
[†]Present address: CTR Carinthian Tech Research AG, Villach, Austria

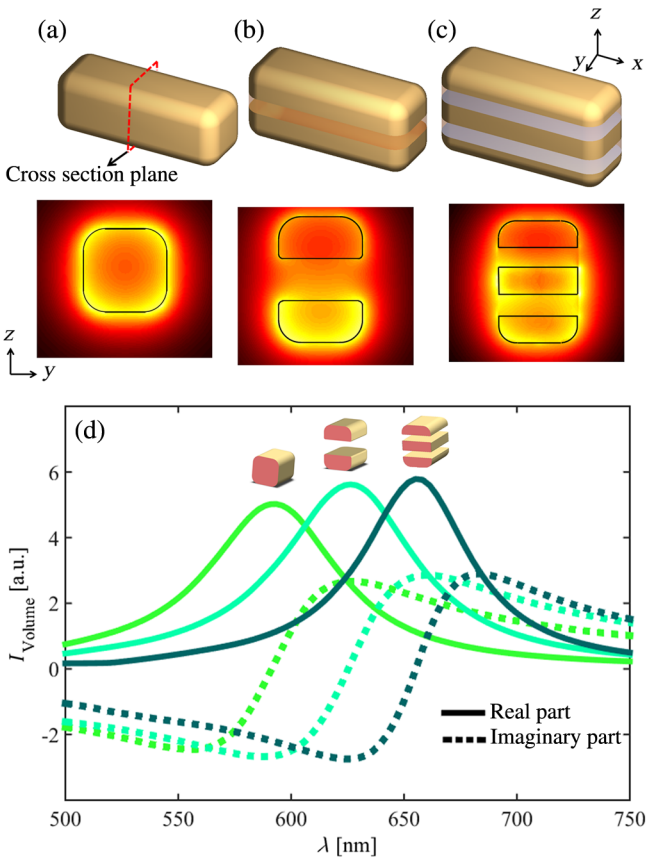


**Fig. 1** (a–c) top: Schematic representation of simple dipole (a), and stratified antennas with (b) two and (c) three metallic layers. For all antennas, the length is 110 nm, the total Au thickness is 40 nm and the spacer material between the metallic layers is air. The propagation vector and the electric field polarization are along the *z*- and *x*-axes, respectively. (a–c) bottom: Calculated electric field intensity in the cross section at the half length for the three antennas at their corresponding resonance wavelengths. (d) Calculated induced volume current through the cross section at half length for the three antennas. Solid line: real part and dashed line: imaginary part.

volume, but their surfaces—especially the segments carrying the maximum current associated with the dipole resonance—increase between (a–c). In this article, we will show both numerically and experimentally that the increase of surfaces that support the plasmonic current associated with a stratified nanoantenna has a strong influence on its radiation properties. The optical measurements are supported by a number of calculations based on the surface integral equation (SIE) method[24] and the influence of the number of interlayers and their thicknesses is studied.

In the stratified antennas shown in Fig. 1, the dielectric spacing between each layer is small and, consequently, the phase difference for the currents flowing in the individual metal layers is negligible for the considered illumination wavelength. However, the total metal/dielectric interfaces for the surface current is increased in the stratified geometries, enhancing the coupling between electrons and photons at those interfaces. This can be seen in Fig. 1(d), where the current $I$ through the cross section of the center for a single-layer, a double-layer, and a triple-layer antenna is calculated, by integrating the current density over the cross section surface $S$

$$I = \oint_{\partial S} \vec{J}(\vec{r}) \cdot \vec{ds}, \tag{1}$$

where $\vec{J}(\vec{r}) = \sigma \vec{E}(\vec{r})$ is the volume current density, $\sigma$ is the conductivity of the material, and $\vec{E}(\vec{r})$ is the electric field. According to these calculations, the current through the central cross section

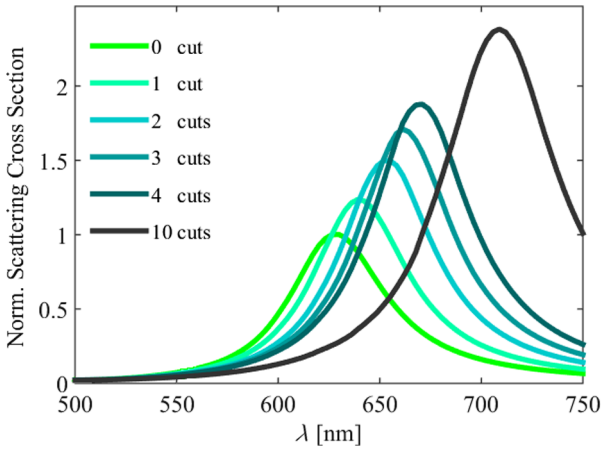


**Fig. 2** Scattering cross section for nanoantenna with zero, 1, 2, 3, 4, and 10 cuts (corresponding respectively to 1, 2, 3, 4, and 11 layers). The spectra have been normalized with respect to the maximum of the spectrum of the single-layer structure. The spacer in each case is air with a thickness of 10 nm.

of the stratified antennas at their corresponding resonance is 12.5% stronger for the double-layer and 16% stronger for the triple-layer antenna as compared to a single-layer antenna. The electric field intensity distributions on the cross sections of the three different antennas [Figs. 1(a)–1(c)] indicate that although the lateral dimensions of the antennas are much smaller than the wavelength and comparable to the penetration depth of the bulk material, the field is not uniform inside the structure and is more concentrated closer to the surface. This indicates that increasing the total surface of a nanoantenna with a given volume and a given resonance length can have a significant influence on its response.

Figure 2 shows the scattering cross sections for antennas with different numbers of horizontal cuts calculated with the SIE.[24] In this figure, an antenna with length, width, and height of 110, 40, and 40 nm, respectively, is cut along its main axis into 2 to 10 pieces. The total height of the metallic parts is kept constant at 40 nm and the spacing between two neighboring parts is 10 nm and filled with air. In practice, the spacing will be filled with a dielectric but here we assume the spacers to be air in order to minimize the spectral shift of the dipole resonance caused by dielectrics.[9] The bulk permittivity of gold has been employed for the metal in the calculations.[25] There are two main trends in these spectra: first, an increase in the maximum of the scattering cross section and, second, the spectrum exhibits a redshift with the number of layers.

As mentioned, the number of layers increases the total surface of the metal, leading to a larger metal/dielectric interface. Consequently, the amount of electrons available for coupling with the photons is increased and the scattering cross section augments. Due to the rapid decay of the electromagnetic field in the metal, the electromagnetic field would be required to penetrate laterally into the spacer medium; hence, the smaller the interlayer the more difficult it is for the field to penetrate into the spacer. Figure 3 represents the scattering cross section spectra for a double-layer antenna with varying spacer thicknesses. According to this figure, the antenna with the largest spacer exhibits the largest scattering cross section. In order to minimize retardation effects, the spacer thickness is kept so small that the phase difference between the upper and the lower dipoles remains negligible and the metallic bars have almost in-phase resonances. For smaller spacers, the region between the upper and the lower layer screens the electromagnetic field and the response of the antenna converges to a conventional one-layer antenna. Let us emphasize that the variation of the scattering cross section for a two-layer antenna with different spacer thicknesses is not as pronounced as for a constant spacer with varying numbers of layers. The intensity of the electric near-field computed for antennas with one, two, and three layers is shown in Fig. 4. The calculations indicate that the maximum near-field intensity for the three cases is almost similar: introducing the interlayers does not produce new hot spots and the response of the structure remains dipolar.[26]

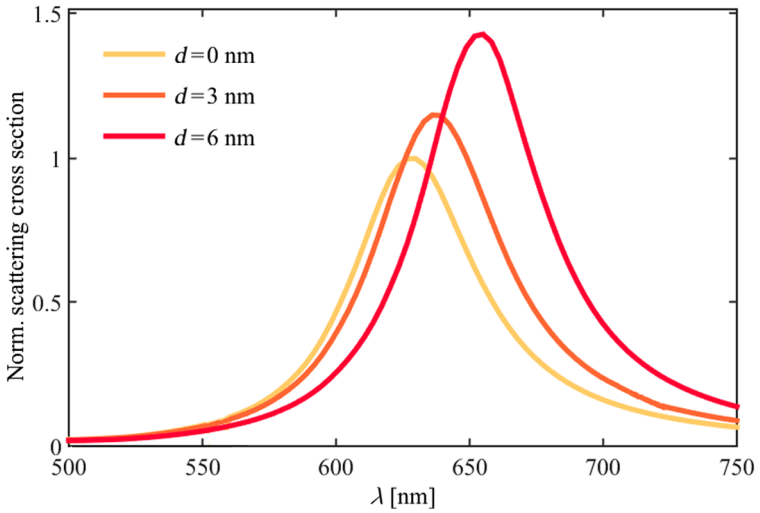


**Fig. 3** Scattering cross section of the antennas with one and two layers. The spectra have been normalized with respect to the maximum of the spectrum of the monolayer structure. The $SiO_2$ spacer thickness varies between 0 and 6 nm.

The redshift of the dipole resonance with increasing numbers of layers is another feature visible in Fig. 2. In order to push further our understanding of the redshift with increasing numbers of layers, the optical response of the antenna can be mimicked by a combination of lumped circuit elements according to the method provided in Ref. 27. A layer of the antenna is represented by two parallel inductive and capacitive branches. As shown in Fig. 5(a), the inductive branch comprises an inductivity $L$ in series with a resistor $R_{ant}$ representing the current path and its associated loss due to the finite metal conductivity. The capacitive branch is composed of a capacitor $C$ in parallel with a resistor $R_{rad}$ representing the fringe field and radiative loss, respectively. The capacitance of the antenna is related to the charge accumulation at both ends of the structure, while the inductance is closely connected to the current flow between both ends. The circuit element values used for this study are as follows: $C = 47$ aF, $L = 2.3$ fH, $R_{rad} = 59.02\ \Omega$, and $R_{ant} = 0.847\ \Omega$.[27] By bringing two antenna layers close to each other, to a distance where phase retardation between the two dipoles is negligible, the dipoles start to interact through the mutual coupling $M$ between the inductors and the coupling capacitors $C_{cp}$, as shown in Fig. 5(b). The capacitor $C_{cp}$ accounts for the pole-to-pole charge interaction and phase retardation and is—under the assumptions made previously—much larger than the dipole capacitor $C$. If the interparticle distance tends to zero, the capacitance $C_{cp}$ goes to infinity, which corresponds to a short cut circuit. Therefore, the circuit can be simplified to four parallel branches: two capacitances $C$ and two inductances $L - M$. As $M > 0$, the resonance frequency shifts from almost $1/\sqrt{LC}$ to higher values $1/\sqrt{(L-M)C}$, corresponding to stronger coupling for small spacers. In Fig. 5(c), the full circuit response of the system with respect to the change in relative mutual inductance is shown. In this case, the capacitances $C_{cp}$ and the loss elements are considered. Increasing the thickness of the

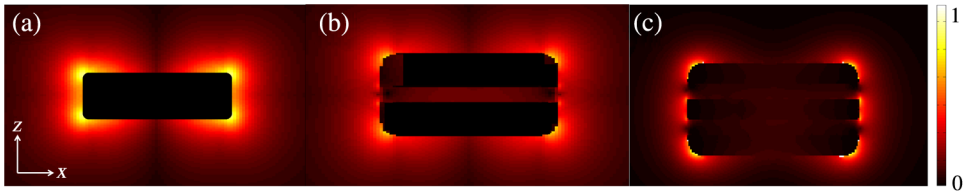


**Fig. 4** Cross section of the antennas in Fig. 1 with the electric field intensity distribution at their resonance wavelength at $y = 0$ nm.

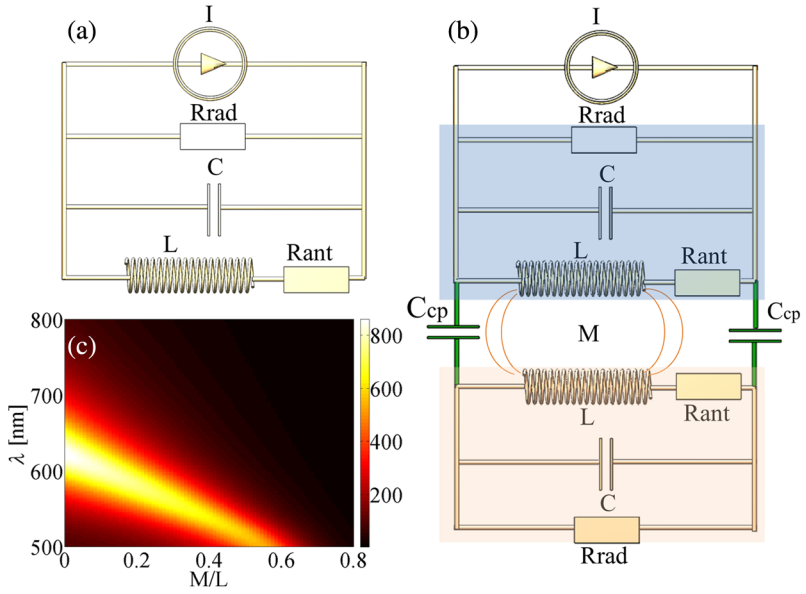


**Fig. 5** Lumped circuit model for (a) a single-layer antenna and (b) a two-layer antenna. (c) Response of the circuit in (b) when changing the amplitude of the mutual inductance *M*.

interlayer and, equivalently, decreasing the relative mutual inductance, enhances the radiation and redshifts the resonance.

In order to provide experimental evidences for the predicted enhancement, arrays of gold nanodisks with diameters of 100, 140, 150, 160, and 170 nm and a pitch of 300 nm were fabricated on a glass substrate using standard electron beam lithography following evaporations and lift-off. The SEM image of a double-layer antenna is shown in Fig. 6(c). For the single-layer antennas, a 1-nm Cr adhesion layer and 40-nm Au were subsequently evaporated. For the double-layer antennas, a bilayer of Cr (1 nm)/Au (20 nm) and a 15-nm spacer of $SiO_2$ and again a bilayer of Cr (1 nm)/Au (20 nm) were evaporated. Optical measurements were performed in transmission with a low numerical aperture 10× objective. Different antenna arrays with the same area were measured and normalized to the direct transmission through the glass substrate without any structure. Figure 6(a) shows extinction (1-transmission)[28] measurements and corresponding SIE periodic calculations[29] for the five arrays of single-layer, respectively double-layer disks in blue, respectively green. According to these results, the fabricated structures have lower and broader extinction in comparison with the calculations; most likely caused by nanofabrication imperfections and the discrepancy between the permittivity used for the calculation and that of the effectively fabricated antennas.[30] However, an enhancement of the extinction, together with a redshift, is clearly visible in that figure when comparing double-layer antennas with single-layer ones [Fig. 6(b)]. In addition, the enhancement is more pronounced for smaller structures and decreases from 28% for 110 nm disks down to 5% for 170 nm disks for the measurements and from 10% to 1.5% for the calculations. This can be attributed to the ratio of the region with penetrated field into the interlayer area to the total increased surface, which decreases for larger structures. Surprisingly, the enhancement observed in the experiment is slightly higher than the enhancement calculated using SIE. This may be related to the inhomogeneity of the evaporation which can cause the formation of many hot spots that can boost the dipolar emission. In that case, the enhancement can be higher for the double-layer antenna since the number of hot spots is larger and the inhomogeneity caused by surface roughness is more pronounced for a 20-nm layer of gold than for a 40-nm layer. In addition, the bulk permittivity of gold used for the calculations might not perfectly match that of fabricated nanostructures. Let us finally mention for the experiments that the thickness of the dielectric layer cannot be excessively thick since an increase of the structure aspect ratio produces pyramidal structures because of the clogging of the lift-off mask during deposition.[31]

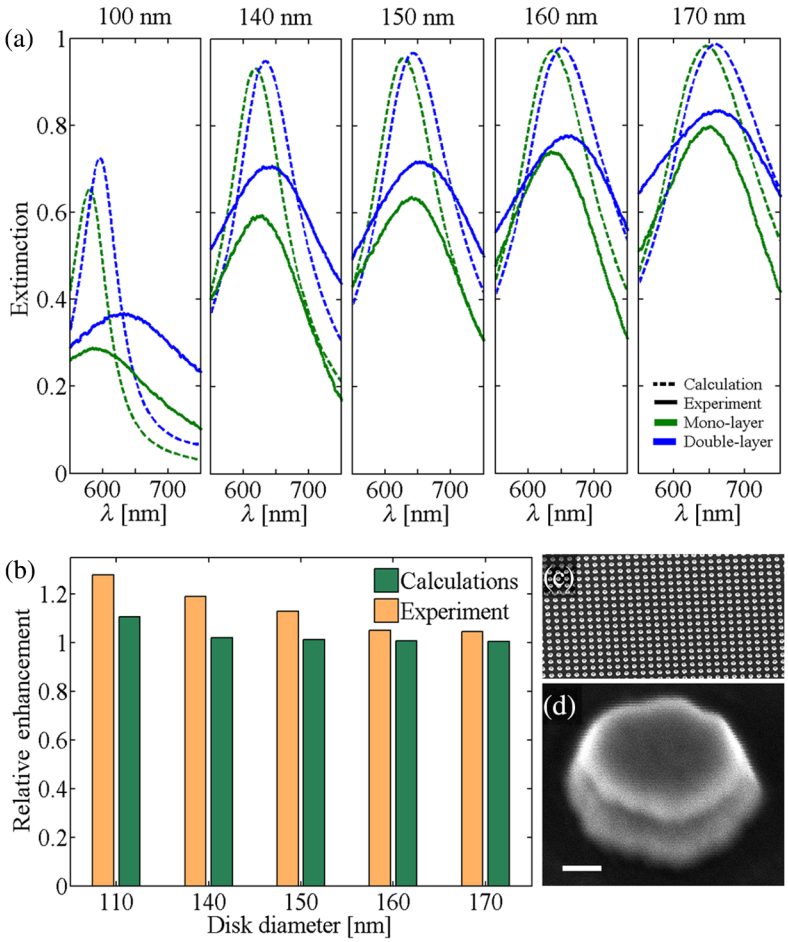


**Fig. 6** (a) Measured extinction spectra (solid lines) and periodic SIE calculations (dashed lines) for the arrays of gold single- (blue) and double-layer (green) disks with the diameters of 110, 140, 150, 160, and 170 nm. The thickness of the single-layer disks as well as the total metal thickness for double-layer disks is 40 nm and the thickness of the intermediate $SiO_2$ spacer is 15 nm. Each array has a period of 300 nm and is realized with electron beam lithography, evaporation, and lift-off. (b) Extinction enhancement percentage for different disk diameters. Green and orange bars represent the calculated and measured enhancement, respectively. (c) SEM image of an array of double-layer nanodisks. (d) SEM image of a double-layer disk. The white color bar corresponds to 40 nm.

## 2 Conclusion

In this study, we have investigated the effect of increasing the total metal/dielectric interface for nanoantennas with a fixed metal volume and a constant length. It has been shown that, although the cross section of the antennas is much smaller than the working wavelength, the interaction between the incoming photons and the metal/dielectric interface of the antenna plays a significant role for the optical response of the antenna. Based on this fact, nanoantennas with a larger number of horizontal cuts (i.e., more number of layers) have shown higher scattering cross sections. By increasing the number of interlayers, the scattering cross section increases. In addition, the penetration of the field into an interlayer with a higher thickness is easier and therefore, the photon–electron interaction for the added surfaces is higher. The far-field enhancement obtained for double-layer structures suggests that in practice, standard single layer deposition can be easily substituted by metal/dielectric/metal deposition, where the thickness of the dielectric is $10 \pm 5$ nm. This approach lends itself to the fabrication of composite plasmonic nanostructures that combine metals and dielectric materials, including semiconductors.[32]

## Acknowledgments

It is a pleasure to acknowledge stimulating discussions with Dr T. V. Raziman. Funding from the European Research Council (ERC-2015-AdG-695206 Nanofactory) is gratefully acknowledged. The authors declare no competing financial interests.

## References

1. T. Klar et al., "Surface-plasmon resonances in single metallic nanoparticles," *Phys. Rev. Lett.* **80**(19), 4249–4252 (1998).
2. J. P. Kottmann and O. J. F. Martin, "Plasmon resonant coupling in metallic nanowires," *Opt. Express* **8**, 655–663 (2001).
3. P. Muhlschlegel et al., "Resonant optical antennas," *Science* **308**(5728), 1607–1609 (2005).
4. K. M. Mayer and J. H. Hafner, "Localized surface plasmon resonance sensors," *Chem. Rev.* **111**(6), 3828–3857 (2011).
5. S. A. Maier, "Plasmonic field enhancement and SERS in the effective mode volume picture," *Opt. Express* **14**(5), 1957–1964 (2006).
6. A. V. Zayats and I. Smolyaninov, "Near-field photonics: surface plasmon polaritons and localized surface plasmons," *J. Opt. A: Pure Appl. Opt.* **5**(4), S16–S50 (2003).
7. A. V. Zayats, I. Smolyaninov, and A. A. Maradudin, "Nano-optics of surface plasmon polaritons," *Phys. Rep.* **408**(3–4), 131–314 (2005).
8. A. M. Kern and O. J. F. Martin, "Excitation and reemission of molecules near realistic plasmonic nanostructures," *Nano Lett.* **11**(2), 482–487 (2011).
9. H. Fischer and O. J. F. Martin, "Engineering the optical response of plasmonic nanoantennas," *Opt. Express* **16**(12), 9144–9154 (2008).
10. A. G. Curto et al., "Unidirectional emission of a quantum dot coupled to a nanoantenna," *Science* **329**(5994), 930–933 (2010).
11. C. Girard et al., "Importance of confined fields in near-field optical imaging of subwavelength objects," *Phys. Rev. B* **50**, 14467–14473 (1994).
12. H. Xu and M. Kall, "Polarization-dependent surface-enhanced Raman spectroscopy of isolated silver nanoaggregates," *ChemPhysChem* **4**(9), 1001–1005 (2003).
13. P. J. Schuck et al., "Improving the mismatch between light and nanoscale objects with gold bowtie nanoantennas," *Phys. Rev. Lett.* **94**(1), 017402 (2005).
14. P. Olk et al., "Two particle enhanced nano Raman microscopy and spectroscopy," *Nano Lett.* **7**(6), 1736–1740 (2007).
15. K. D. Alexander et al., "A high-throughput method for controlled hot-spot fabrication in SERS-active gold nanoparticle dimer arrays," *J. Raman Spectrosc.* **40**(12), 2171–2175 (2009).
16. W. H. Zhang et al., "Mode-selective surface-enhanced Raman spectroscopy using nanofabricated plasmonic dipole antennas," *J. Phys. Chem. C* **113**(33), 14672–14675 (2009).
17. W. Y. Li et al., "Dimers of silver nanospheres: facile synthesis and their use as hot spots for surface-enhanced Raman scattering," *Nano Lett.* **9**(1), 485–490 (2009).
18. N. A. Hatab et al., "Free-standing optical gold bowtie nanoantenna with variable gap size for enhanced Raman spectroscopy," *Nano Lett.* **10**(12), 4952–4955 (2010).
19. D. K. Lim et al., "Nanogap-engineerable Raman-active nanodumbbells for single-molecule detection," *Nat. Mater.* **9**(1), 60–67 (2010).
20. M. Rycenga et al., "Understanding the SERS effects of single silver nanoparticles and their dimers, one at a time," *J. Phys. Chem. Lett.* **1**(4), 696–703 (2010).
21. K. D. Osberg et al., "Dispersible surface-enhanced Raman scattering nanosheets," *Adv. Mater.* **24**(45), 6065–6070 (2012).
22. J. B. Herzog et al., "Dark plasmons in hot spot generation and polarization in interelectrode nanoscale junctions," *Nano Lett.* **13**, 1359–1364 (2013).
23. L. Tong, H. Xu, and M. Kall, "Nanogaps for sers applications," *MRS Bull.* **39**, 163–168 (2014).
24. A. M. Kern and O. J. F. Martin, "Surface integral formulation for 3D simulations of plasmonic and high permittivity nanostructures," *J. Opt. Soc. Am. A* **26**(4), 732–740 (2009).

25. P. B. Christy and R. W. Johnson, "Optical constants of transition metals: Ti, V, Cr, Mn, Fe, Co, Ni, and Pd," *Phys. Rev. B* **9**(12), 15 (1974).
26. J. P. Kottmann et al., "Field polarization and polarization charge distributions in plasmon resonant nanoparticles," *New J. Phys.* **2**, 27 (2000).
27. B. Abasahl, C. Santschi, and O. J. F. Martin, "Quantitative extraction of equivalent lumped circuit elements for complex plasmonic nanostructures," *ACS Photonics* **1**, 403–407 (2014).
28. C. F. Bohren and D. R. Huffman, *Absorption and Scattering of Light by Small Particles*, John Wiley & Sons, New York (1983).
29. B. Gallinet, A. M. Kern, and O. J. F. Martin, "Accurate and versatile modeling of electromagnetic scattering on periodic nanostructures with a surface integral approach," *J. Opt. Soc. Am. A* **27**, 2261–2271 (2010).
30. W. Haiss et al., "Determination of size and concentration of gold nanoparticles from UV-vis spectra," *Anal. Chem.* **79**(11), 4215–4221 (2007).
31. Y. Ekinci et al., "Electric and magnetic resonances in arrays of coupled gold nanoparticle in-tandem pairs," *Opt. Express* **16**, 13287–13295 (2008).
32. H. Wei and H. Xu, "Plasmonics in composite nanostructures," *Mater. Today* **17**(8), 372–380 (2014).